Structure of $LiAl_2(OH)_7 \cdot 2H_2O$

J. P. Thiel, C. K. Chiang, and K. R. Poeppelmeier*

Department of Chemistry and Ipatieff Catalytic Laboratory, Northwestern University, Evanston, Illinois 60208

Received August 28, 1992. Revised Manuscript Received December 14, 1992

The room-temperature reaction of lithium hydroxide with aluminum hydroxide (bayerite) in the ratio of 1:2 produces lithium dialuminate, $LiAl_2(OH)_7 \cdot 2H_2O$. Rietveld refinement of X-ray and neutron powder diffraction patterns indicate that the structure is composed of $[LiAl_2(OH)_6]^+$ layers separated by water molecules and hydroxide ions. Disorder in the stacking sequence leads to indexing the diffraction pattern on a hexagonal cell (a = 5.0972(3) Å, c = 7.5524(9) Å × $3n$ layers); however, the structure is better described by a C-centered monoclinic cell with the constraints the $b = a\sqrt{3}$ and $\cos\beta = -a/3c$ (a = 5.097 Å, b = 8.829 Å, c = 7.741 Å, and β = 103.0°). The diffraction patterns were refined using a model of up to 54 layers (~400 Å). The layer stacking vector, which defines the angle between layers, is less than expected based on the position of the diffraction peaks. The structural complexities present in lithium dialuminate have their origins in the conditions of synthesis and the layered nature of the material.

Introduction

Mixed metal hydroxides with layer structures form a class of compounds related to clays.[1-4] These materials consist of positively charged metal hydroxide sheets between which anions and water molecules are located. The natural carbonate–hydroxide of magnesium and aluminum occurs in two different structures, rhombohedral hydrotalcite and hexagonal manasseite. While both phases are commonly intergrown, manasseite generally forms the core and hydrotalcite the outer part of the grain. Hydrotalcite appears to form later than the coexisting manasseite phase and, presumably, at lower temperatures. Artificially synthesized hydrotalcite-like compounds have been studied extensively.[5-8] The principle areas of interest are catalyst supports, anion exchange materials, fire retardant materials, and as a catalyst precursor for high surface area α-$LiAlO_2$.[9,10]

The mineral hydrotalcite, $[Mg_3Al(OH)_8]_2(CO_3)\cdot 2H_2O$, can be thought of as composed of $Mg(OH)_2$ (brucite) layers, in which each Mg^{2+} cation is surrounded by six hydroxyl groups in an octahedral arrangement. These octahedra share edges to form sheets. When an Al^{3+} cation replaces a Mg^{2+} cation, each layer gains a positive charge which is balanced by interlayer anions. The interlayer species can be easily ion exchanged. Related hydrotalcite-like phases can be expressed by $[(M^{2+})_{1-x}(M^{3+})_x(OH)_2]^{x+}(A^{-m})_{x/m}\cdot nH_2O$, where M^{2+} = Mg, Ni, Fe; M^{3+} = Al, Cr; A^{m-} = OH^-, Cl^-, CO_3^{2-}, and x ranges between 0.20 and 0.33.

The general formula of hydrotalcite can be extended if M^{2+} is replaced by M^+. Serna et al. first obtained the hydrotalcite-like compound using monovalent lithium cation with the composition $[LiAl_2(OH)_6]_2(CO_3)\cdot nH_2O$.[11] As in natural hydrotalcite, this Li–Al hydroxycarbonate comprises $Al(OH)_3$ layers, in which the empty octahedral sites left by Al^{3+} cations are occupied by the Li^+ cations, resulting in a positively charged layer that requires an interlayer anion for charge balance. To date, the structure and ion-exchange behavior of these materials remain relatively unexplored.[12] In this paper we report the detailed structural characterization of $[LiAl_2(OH)_6]^+OH^-\cdot 2H_2O$ prepared by the room-temperature reaction of $Al(OH)_3$ with $LiOH\cdot H_2O$ (salt imbibition).

Experimental Section

Previous work[13] involved the preparation of chemically modified solid precursors by a salt imbibition technique.[14] Anions other than carbonate were considered. Lithium hydroxide and lithium nitrate were imbibed into layered $Al(OH)_3$ at room temperature. The synthesis is easy to carry out and is an improvement over the conventional solution process because the problem of incomplete reaction can be overcome by the direct reaction of the lithium salt with polycrystalline $Al(OH)_3$ in the solid state. These solids readily react when placed together and exposed to water vapor.[13] For example, 0.5 g (6.4×10^{-3} mol) of dried bayerite and 0.1348 g (3.2×10^{-3} mol) of $LiOH\cdot H_2O$ were mixed by grinding in an alumina mortar. The mixture was placed in a glass tube under flowing water-saturated nitrogen gas at room temperature for several days. Other hydrotalcite-like phases can be prepared by an analogous method. The reaction does not occur if the carrier gas is dry air or dry nitrogen. The final composition has one hydroxyl anion and two water molecules incorporated into the structure, as determined by thermogravimetric analysis. Excess water was initially found on the solid but can be removed by vacuum drying at room temperature. Presumbly, water molecules reside on the surface and inside pores

(1) Allmann, R. *Chimia* **1970**, *24*, 99.
(2) Miyata, S. *Clays Clay Miner.* **1980**, *28*, 50.
(3) Miyata, S. *Clays Clay Miner.* **1983**, *31*, 305.
(4) Reichle, W. T. *Solid State Ionics* **1986**, *22*, 135.
(5) Ulibarri, M. A.; Hernandez, M. J.; Cornejo, J. *J. Mater. Chem. Phys.* **1986**, *14*, 209.
(6) Brindley, G. W.; Kikkawa, S. *Clays Clay Miner.* **1980**, *28*, 87.
(7) Hernandez, M. J.; Ulibarri, M. A.; Rendon, J. L.; Serna, C. *J. Phys. Chem. Miner.* **1985**, *12*, 34.
(8) Dutta, P. K.; Puri, M. *J. Phys. Chem.* **1989**, *93*, 376.
(9) Poeppelmeier, K. R.; Chiang, C. K.; Kipp, D. O. *Inorg. Chem.* **1988**, *27*, 4523.
(10) Tomczak, D. C.; Thong, S. H.; Poeppelmeier, K. R. *Catal. Lett.* **1992**, *12*, 139.
(11) Serna, C. J.; White, J. L.; Hem, S. L. *Clays Clay Miner.* **1977**, *25*, 384.
(12) Sissoko, I.; Iyagba, E. T.; Sahai, R.; Biloen, P. *J. Solid State Chem.* **1985**, *60*, 283.
(13) Poeppelmeier, K. R.; Hwu, S.-J. *Inorg. Chem.* **1987**, *26*, 3297.
(14) Glasstone, S. *Textbook of Physical Chemistry*; Macmillan & Co.: London, 1956; Vol. 12, p 1259.

0897-4756/93/2805-0297$04.00/0

and assist the salt imbibition by interparticle diffusion of lithium hydroxide.

The powder X-ray diffraction pattern of $LiAl_2(OH)_7{\cdot}2H_2O$ was collected using Cu Kα radiation filtered with nickel foil on a Rigaku diffractometer which employs a Bragg-Brentano geometry. Data were collected at room temperature by step scanning over the range $9° \leq 2\theta \leq 80°$ in increments of 0.02°. Multiple data collections were required. Initial analysis of the data indicated a serious problem with the intensity ratio of the (003) and (006) peaks when the dispersion slit was too wide such that some of the incident beam missed the sample at low angle. The relative intensity of the (003) reflection in previously published work[13] is ~30% too low. To determine peak intensities, small portions of the pattern were fit using a nonlinear least squares program (a Marquet method after Bevington[15]) to pseudo-Voigt shaped peaks according to eq 1. σ_K is the peak width of the *Kth* reflection. Simulated intensities where generated by Lazy-Pulverix[16] and plotted with pseudo-Voigt shaped peaks that had a width of 0.15° 2θ and η of 0.5.

$$P_{i_K} = \eta\frac{2}{\pi\sigma_K}\left[1/\left(1+4\frac{(2\theta_i-2\theta_K)^2}{\sigma_K{}^2}\right)\right] + (1-\eta)\frac{8(\ln 2)^{1/2}}{\pi^{1/2}\sigma_K}e^{-4\ln 2(2\theta_i-2\theta_K)^2/\sigma_K{}^2} \quad (1)$$

$$P_{i_K} = 0 \text{ for } (2\theta_i - 2\theta_K)^2 > (C_{\text{limit}}\sigma_K)^2$$

A time-of-flight neutron data set was collected at room temperature at the intense pulse neutron source (IPNS) facility at Argonne National Laboratory. The sample used to acquire the neutron pattern was prepared by hydrothermal exchange of $LiAl_2(OH)_7{\cdot}2H_2O$ with D_2O. The deuerium to hydrogen ratio is approximately 3:1. A small amount of a lithium-rich second phase (Li/Al ~6) was detected in the X-ray powder pattern. It has not yet been isolated as a single phase. The four most intense peaks are at 21.3° (100%), 30.6° (70%), 31.8° (95%), and 34.1° (40%). Only the two most intense peaks are weakly visible in the diffraction patterns, and the phase is neglected in the refinements.

Results and Discussion

Basic Structure. The bayerite structure is monoclinic,[16,17] but the distortion from hexagonal symmetry is relatively slight and can be approximated with a pseudo-hexagonal cell in which $a \approx 5.1$ Å and $c \approx 4.7$ Å.[13] In $Al(OH)_3$ the aluminum cations occupy two-thirds of the octahedral sites between sheets of close-packed hydroxyl anions. After salt imbibition, the lithium cations presumably fill the remaining octahedral sites and the unit cell expands in the direction perpendicular to the bayerite plane to accommodate the two water molecules and one hydroxide ion per formula unit. The amount of expansion, 2.8 Å per layer, is the appropriate size for a layer of imbibed hydroxide ions and water molecules. A hexagonal unit cell was used to index the X-ray and neutron powder diffraction patterns with parameters $a = 5.103(1)$ Å and $c = 22.674(8)$ Å (Figure 1).[13] The intralayer cell parameters α and γ associated with the intralayer dimensions are unaffected by the reaction so it is reasonable to assume that any distortions are slight. It has been proposed, based on the ion-exchange chemistry, that the lithium occupies the vacant octahedral sites in the bayerite framework.[19]

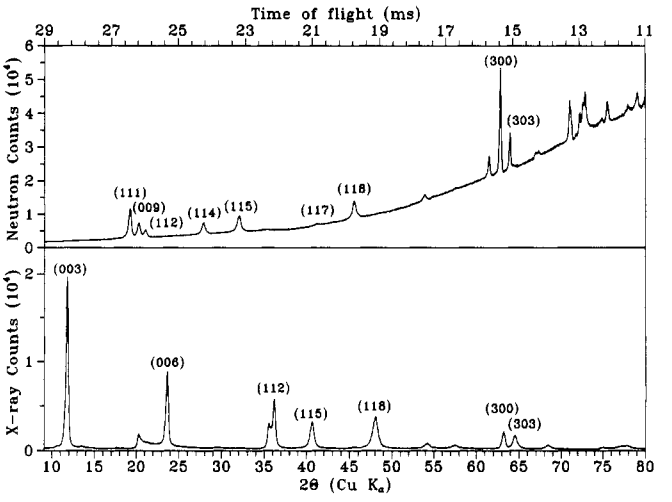

Figure 1. Neutron (above) and X-ray (below) diffraction patterns of $LiAl_2(OH)_7{\cdot}2H_2O$ with some important reflections labeled.

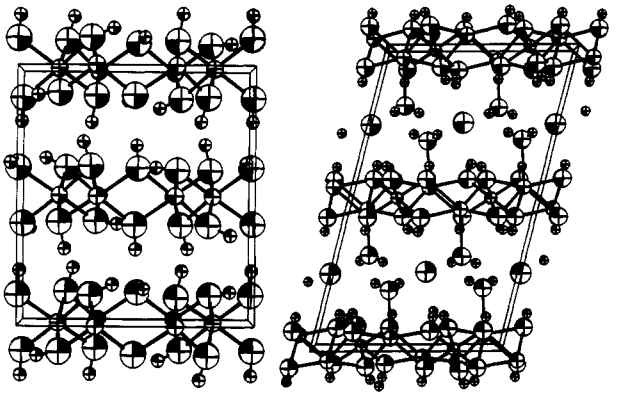

Figure 2. ORTEP drawings of Bayerite (left) and $Ca_2Al(OH)_6Cl{\cdot}2H_2O$ (right). The size of atoms reflects crystal radius rather than thermal vibrations.

The lithium atom position will not have a strong impact on the diffraction intensities since the difference between[19] a vacancy and lithium atom (3 e$^-$) is small compared with two aluminum atoms (26 e$^-$) and the number of electrons per $[LiAl_2(OH)_6]^+OH^-{\cdot}2H_2O$ unit (112 e$^-$). The tripling of the c axis has been examined carefully[13] against two major peaks at $2\theta = 40.5°$ and $2\theta = 48.0°$ that cannot be indexed unless a triple layer unit cell is employed. The Bragg reflections with $L \neq 3n$ also indicte a tripled c axis is the repeat unit.

Relationship to $[Ca_2Al(OH)_6]^+Cl^-{\cdot}2H_2O$. To derive a structure based solely on powder diffraction data is a difficult undertaking. As much as possible, the known chemistry should be consistent with the proposed structure. A search of hydrotalcite stoichiometries with structural data produced one possibly related compound, $Ca_2Al(OH)_6Cl^-{\cdot}2H_2O$. It has the same charge density and number of intercalated species and the anions are approximately close packed. The structure of this compound was reported by Burzlaff et al.[20,21] and is compared with that of bayerite in Figure 2. A comparison of the simulated powder patterns of this and other close-packed models

(15) Bevington, P. *Data Reduction and Error Analysis for the Physical Sciences*; McGraw-Hill: New York, 1969.
(16) Yvon, K.; Jeitschko, W.; Parthe, E. Lazy-Pulverix, Laboratoire de Crystallographie, Aux Rayon-X, Univ. Geneve, Geneva, Switzerland, 1977.
(17) Rothbauer, V. R.; Zigan, F.; O'Daniel, H. Z. *Kristallogr.* **1967**, *125*, 317.
(18) Zigan, F.; Joswig, W.; Burger, N. Z. *Kristallogr.* **1978**, *148*, 255.
(19) Sissoko, I.; Iyagba, E. T.; Sahai, R.; Biloen, P. *J. Solid State Chem.* **1985**, *60*, 283.
(20) Terzis, A.; Filippakis, S.; Kuzel, H. J.; Burzlaff, H. Z. *Kristallogr.* **1987**, *181*, 29.
(21) In the previous reference, two typographical errors are present in the table of atom positions. X of O(2) is 0.052 96 not 0.529 60 and Y of O(3) is 0.820 10 not 0.082 01.

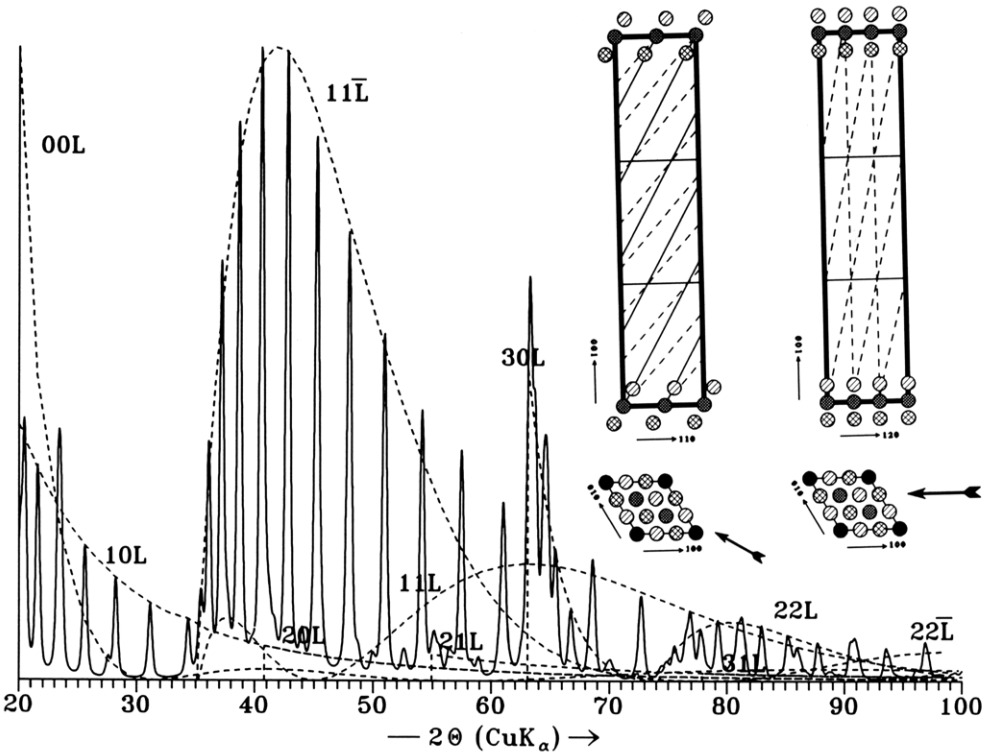

Figure 3. Simulated X-ray diffraction pattern of one $LiAl_2O_6$ layer per unit cell. ● and ● represent lithium and aluminum atoms. ⊗ and ⊘ represent oxygen atoms above and below the metal atom plane.

did not reveal any obvious similarity. There are some structural elements present in the calcium structure that cannot be present in the dialuminate. The larger calcium cation expands the ab plane to 5.2 Å on an edge relative to 5.1 Å in the dialuminate. The calcium ion is seven-coordinate including the intercalated water molecule. This type of bonding cannot be present in the dialuminate because the plane does not expand and the aluminum and lithium have considerably smaller ionic radii. This further explains the stability of the calcium compound where crystals form under hydrothermal conditions at 200 °C. The dialuminate decomposes at much lower temperatures.

Structural Models. The hexagonal indexing[13] accounts for the observed reflections, but the number of unobserved reflections is cause for concern with less than two dozen observable reflections while there are 69 atoms per unit cell. Therefore, many of the atoms must be located on symmetric or nearly symmetric sites. One might expect that the distortion from a single layer cell would be small and the (*HKL*) reflections with $L \neq 3n$ should have near zero intensity. Models based on close packed oxygen atoms all produce strong reflections for $L = 3n$. In contrast, the observed pattern is quite different. The third and fourth most intense peaks are indexable as the (118) and (115), respectively, while the (113), (116), and (119) (those with $L = 3n$) are extremely weak. The (115) and (118) are strong reflections, so strong that the $LiAl_2O_6$ layers must constructively contribute since they account for approximately 75% of the total electron density.

To begin to develop a structural model, the theoretical X-ray powder pattern of a single layer of $LiAl_2O_6$ in the unit cell was calculated (Figure 3). The scattering owing to different *HK* reflection sets, shown as dashed ines, was modeled with a single $LiAl_2O_6$ layer in an arbitrarily large (>100 Å) cell. As expected, the scattering is strong for the (11*L*) reflections and it is the (11$\bar{L}$) reflections that are responsible. Therefore a structure composed of these $LiAl_2O_6$ units will result in destructive interference of the single layer diffraction pattern.

Atomic Positions. The relative positions of the two remaining $LiAl_2O_6$ layers must be chosen so that they constructively interfere for the (11$\bar{5}$) and (11$\bar{8}$) and are located at roughly $^1/_3$ and $^2/_3$ along the *z* axis. Figure 3 shows the projection of the first $LiAl_2O_6$ layer, centered at $z = 0$ where each circle represents a column of atoms. Also marked are the (11$\bar{5}$) and (11$\bar{8}$) Bragg planes and the $z = {}^1/_3$ and $^2/_3$ levels. This viewing direction is useful because the Bragg planes of interest appear as lines and their intersection occurs at $^1/_3 + {}^n/_2$ (*n* is an integer) the distance across the 110 direction for $z = {}^1/_3$. The condition is then that $\Delta X + \Delta Y = {}^2/_3 + n$. To completely determine ΔX and ΔY, a second family of reflections must be considered. The (300) and (303) reflections are strong and the same argument as for the (11*L*) applies. The projection also shows the (300) and (303) Bragg planes. They intersect at ΔX (or ΔY) equal to $^n/_3$. Combining these criteria, there appear to be three possibilities for the vector between successive layers [$^1/_3$,$^1/_3$,$^1/_3$], [0,$^2/_3$,$^1/_3$], and [$^2/_3$,0,$^1/_3$]. These are equivalent and correspond to 120° rotations of the unit cell axes. Figure 4 shows the calculated X-ray powder pattern for this model. The desired peaks are present and strong if not at the correct relative intensities.

The positions of the three interlayer oxygens (from the hydroxide and water molecules) were determined in the same manner as the $LiAl_2O_6$ units. The (111), (11$\bar{2}$), and (11$\bar{1}$0) were underestimated relative to the (11$\bar{5}$) and (11$\bar{1}\bar{1}$) reflections by the model in Figure 4. We take the same approach as with the layers to determine the positions of the intercalated atoms. But there is an additional complication, that is the (11*L*), (2$\bar{1}$*L*), and (1$\bar{2}$*L*) reflections are not equivalent as they would be if the structure was truly hexagonal. The solid lines represent the reflections

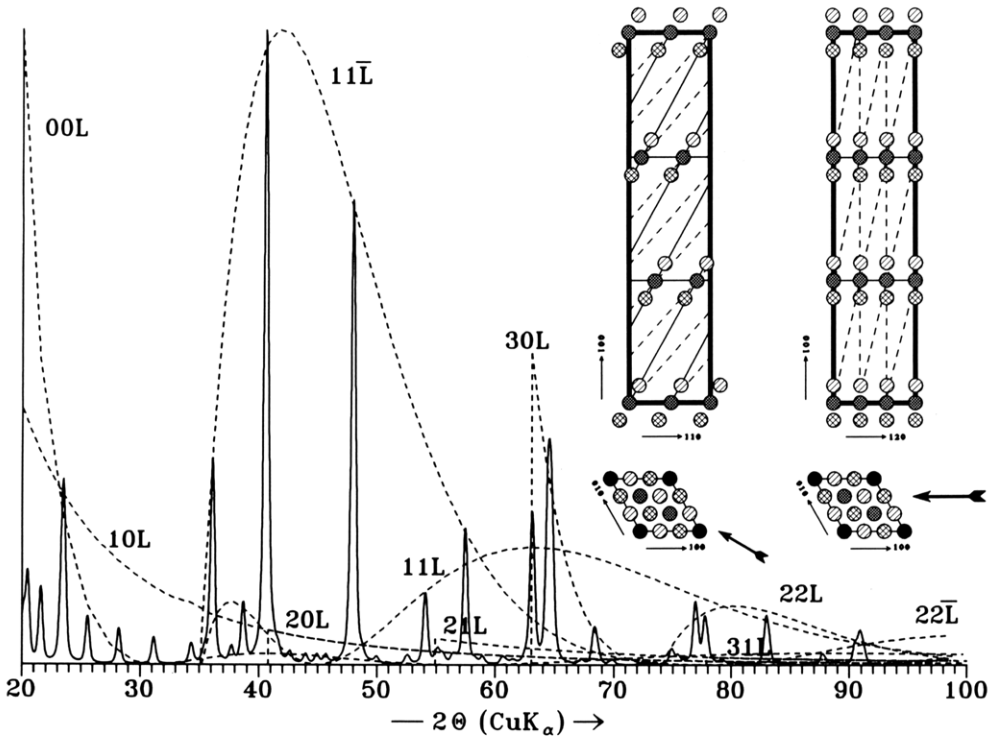

Figure 4. Simulated X-ray diffraction pattern of three $LiAl_2O_6$ layers per unit cell.

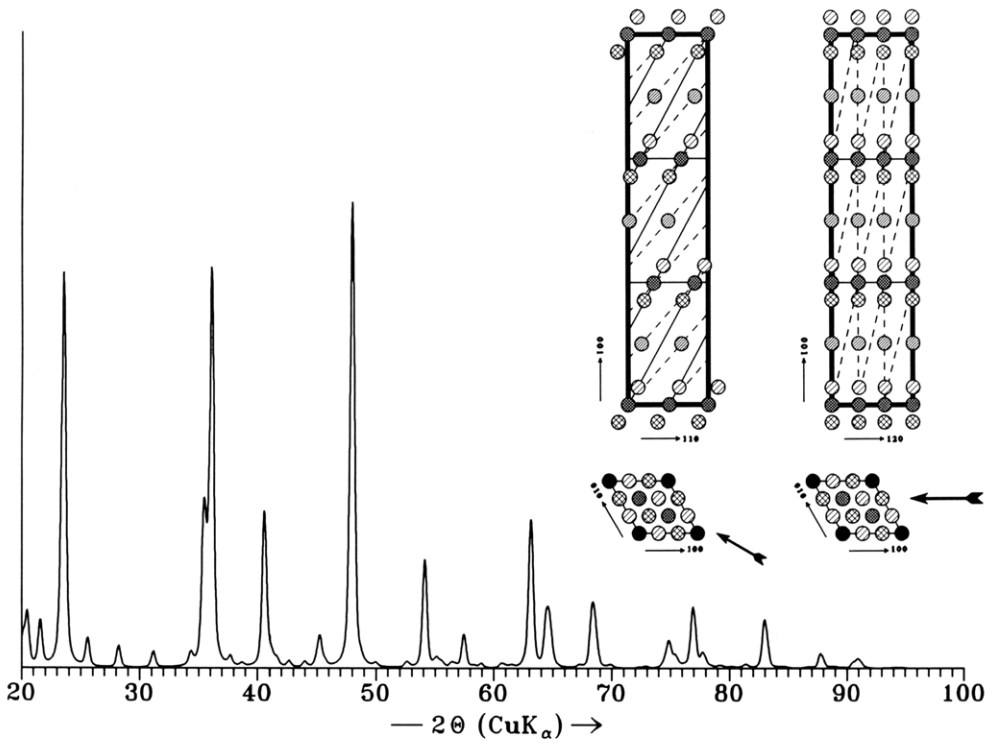

Figure 5. Simulated X-ray diffraction pattern including interlayer oxygen species.

that are stronger in the observed pattern than in the calculated, while the dashed represent those that are weaker. From this we estimate the interlayer oxygens to be located at ($^1/_6$,$^1/_6$,$^1/_6$), ($^1/_2$,$^5/_6$,$^1/_6$), and ($^5/_6$,$^1/_2$,$^1/_6$) and at the same relative positions between the other layers, +($^1/_3$,$^1/_3$,$^1/_3$) and +($^2/_3$,$^2/_3$,$^2/_3$). The calculated pattern is shown in Figure 5. The error in the relative intensities is now reversed, and the ($11\bar{5}$) is too small relative to the ($11\bar{8}$) and ($11\bar{2}$). Nonetheless the pattern is quite similar to the observed pattern. Another iteration of this procedure suggests displacing the intercalated atoms slightly, $\Delta X, \Delta Y \approx -0.03$. At this point locations for all the atoms, except hydrogens, have been chosen, and, because relatively small displacements are being considered, the model is sufficiently determined that it can be analyzed using the Rietveld method. The Rietveld method requires a space group as well as atom positions and a unit cell. The choice of space group can be avoided by using $P1$ and determining the approximate symmetry by coupling the shifts of the atomic positions. This brings up the question of the correct unit cell.

Unit Cell Size. The staggering of the layers means that the structure is not hexagonal despite the observation that all the observed reflections can be indexed on such

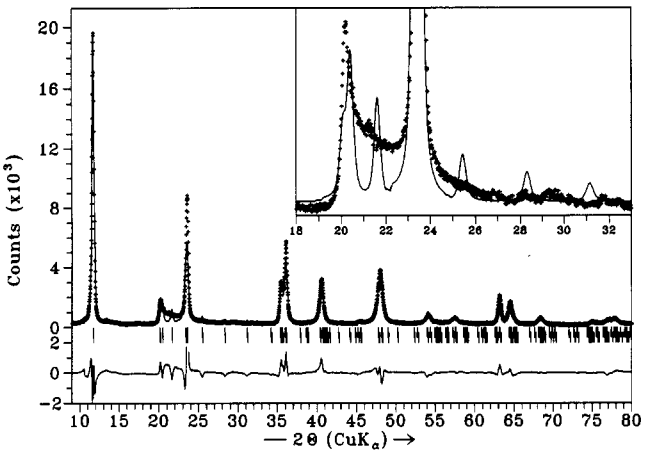

Figure 6. Rietveld refinement of $LiAl_2(OH)_7{\cdot}2H_2O$ in $C2/m$.

a cell. A smaller C-centered monoclinic cell can be formed from the triple layer cell by the matrix:

$$\begin{bmatrix} a \\ b \\ c \end{bmatrix}_{hex} \begin{bmatrix} 1 & 1 & 0 \\ 1 & -1 & 0 \\ \frac{1}{3} & \frac{1}{3} & \frac{1}{3} \end{bmatrix} = \begin{bmatrix} a \\ b \\ c \end{bmatrix}_{mono} \quad (2)$$

We will continue to describe the cell in terms of our original model since it is easier to visualize in much the same way that an fcc lattice is easier to picture as a cube than the primitive rhombohedron. The smaller cell will be used for Rietveld refinement. This is done for $C2/m$, the highest possible symmetry in the monoclinic setting. The result is shown in Figure 6.

The region of the powder pattern with the largest deviation relative to the calculated pattern is from 19° to 32°. The calculared peaks in this region are ($10L$) reflections in addition to the (006). There is a sharp onset just below 20° 2θ and then a gradual and uniform decrease in intensity which doesn't reach the initial background until at least 26°. This is intrinsic to the material, not an instrumental effect, and reproducible in every preparation. The ($10L$) reflections are crucial to answering the question of the lithium site. The intensities calculated for the ($10L$) reflections result from the difference in scattering of lithium versus that of aluminum and the expansion of the coordination sphere around the larger lithium ion. The ($10L$) lines would be systematically extinct for a random occupation of the three metal sites in the $LiAl_2O_6$ layer. With the current unit cell, there are only a few reflections in this region and no amount of line broadening can generate the observed peak's asymmetric shape. This is further reflected in the atomic parameters of $C2/m$ refinement and a less constrained refinement in $P\bar{1}$ listed in Table I. The thermal parameters are not physically meaningful because the effect of site occupancy and thermal parameters is to produce a large difference at low angle and little difference in scattering at higher angles to follow the asymmetric region as well as possible.

The model cannot account for all the diffraction intensity in the region between 20° and 26°. A small contribution is made by the lithium-rich impurity (the peaks at 21 and 29°) but not the majority of the intensity. A more complex ordering of the lithium positions from one layer to the next would generate a supercell and intermediate reflections in the region. The rest of the pattern would be largely unaffected by any ordering of metal atoms. For the ($00L$), ($11L$), ($30L$), and ($22L$) reflections, the metal sites in the $LiAl_2O_6$ layers project onto each other so that only the average electron density is important. The size of a supercell must be relatively large, a minimum number appears to be approximately 8–10 layers. This large cell generates sufficient overlapping reflections that can not be observed discreetly. Extended ordering does not seem reasonable in a material with poor crystallinity as evidenced by the breadth of the observed peaks. The peak width is a measure of the effective particle size. According to the Scherrer formula: $t = 0.6\lambda/B \cos\theta_B$ where t is the thickness, θ_B is the angle of the reflection and B is the degree of broadening in radians relative to a highly crystalline standard. The width of the (006) reflection indicates an effective thickness of ~150 Å or 20 layers, or in other words the "unit cell" is the effective length of the crystallite. Therefore the stacking is random and does not distinguish between lithium and aluminum positions and, as noted before, there are three equivalent positions when choosing the position of the next layer. The relative position of one lithium to those above and below is random with (ΔX,ΔY) either ($^1/_3$,$^1/_3$), ($^2/_3$,0) or (0,$^2/_3$). The imbibition reaction does not maintain the long-range ordering of the layers as the lithium cations, hydroxide anions, and water molecules diffuse in from the crystallite edge separating the layers. The effect is similar to stacking faults in close packed structures. Owing to crystal growth conditions,[22] martensitic phase transitions,[23] or plastic deformations,[24] some layered systems are known to transform to partially ordered systems alternating between hcp and ccp type stacking.

Table I. Refined Unit Cell and Atomic Parameters in $P\bar{1}$ and $C2/m$

atom	site	X	Y	Z	B
Li	$1a, \bar{1}$	0	0	0	− 9.6
Al	$2i, 1$	0.337	0.690	0.000	7.7
O(1)	$2i, 1$	0.312	0.951	0.149	4.7
O(2)	$2i, 1$	0.953	0.229	0.125	1.4
O(3)	$2i, 1$	0.625	0.604	0.136	4.8
O(4)	$1h, \bar{1}$	$^1/_2$	$^1/_2$	$^1/_2$	8.7
O(5)	$2i, 1$	0.209	0.875	0.506	12.5
	a = 5.095 Å, b = 5.093 Å, c = 7.7576 Å, α = 83.17°, β = 83.73°, γ = 119.93°				
Li	$2a, 2/m$	0	0	0	− 7.9
Al	$4g, 2$	0	0.335	0	2.3
O(1)	$8j, 1$	0.866	0.181	0.134	− 1.8
O(2)	$4i, m$	0.397	0	0.142	1.9
O(3)	$2d, 2/m$	0	$^1/_2$	$^1/_2$	1.1
O(4)	$4h, 2$	0	0.155	$^1/_2$	7.7
	a = 5.097 Å, b = 8.828 Å, c = 7.718 Å, β = 102.7°				

The scattering owing to disordered stacking of layered materials was addressed many years ago by Teller[25] among others.[26,27] The scattering is described by equation 3. L is the particle length and θ_0 is the location of the peak for

$$I(\theta) = \frac{1 + \cos(2\theta)}{\sin^2\theta \cos\theta} \int_0^\infty \exp\{-[x^2 - (2\sqrt{\pi}L/\lambda)(\sin\theta - \sin\theta_0)]^2\}\, dx \quad (3)$$

(22) Zachariasen, W. H. *Acta Crystallogr.* **1948**, *1*, 277.
(23) Edwards, O. S.; Lipson, H. *Proc. R. Soc.* (London) **1942**, *39A*, 268.
(24) Barrett, C. S. *Phys. Rev.* **1951**, *81*, 311.
(25) Teller, E.; Hendricks, S. *J. Chem. Phys.* **1942**, *10*, 147.
(26) Warren, B. E. *Phys. Rev.* **1941**, *59*, 693.
(27) Zachariasen, W. H. *Phys. Rev.* **1947**, *71*, 715.

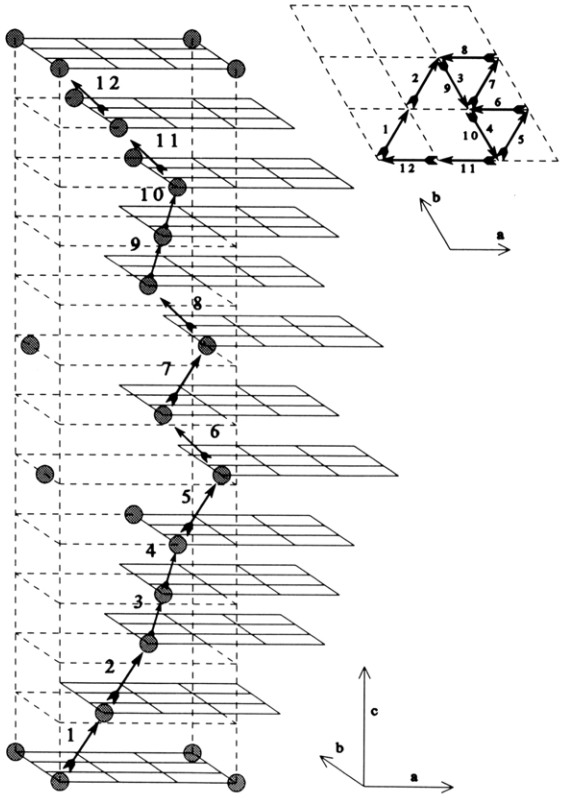

Figure 7. Schematic drawing of a 12-layer model. Only lithium atoms are shown to indicate the shifts.

an ordered material (the 100 Bragg reflection in the lithium dialuminate case). The diffraction for $LiAl_2(OH)_7{\cdot}2H_2O$ is more complicated because multiple atoms contribute to the scattering from each $[LiAl_2(OH)_6]^+$ layer. The expansion of the oxygen atoms around the lithium cation strongly affects the diffuse intensity owing to plane scattering, as well as the Bragg peaks; therefore, it is not possible to decouple the two. A random stacking sequence does explain the original hexagonal unit cell parameters, when the staggering of the layers would be expected to produce a monoclinic system ($b = a\sqrt{3}$ and $\cos\beta = -a/3c$). The pseudohexagonal symmetry results when small deviations are averaged out by the random stacking of the layers.

Twelve-Layer Model. With no way to readily account for the interference between the oxygen and metal ions in the diffuse scattering, modelling the random stacking poses a problem. A thorough approach would be to generate a large number of different stacking sequences, calculate the intensity in reciprocal space, convolute the Fourier transform of an appropriate shape function for each particle, determine how reciprocal space will map to the observed intensity for our diffractometer, and finally add all the components together. All of which is far too computationally involved. Available programs are designed to calculate the ideal structure and then use a smoothly varying peak shape function to account for the shape function and diffractometer. A reasonable approximation could be made by using a model so large in the c axis that the oscillations associated with the model are the same magnitude as the noise associated with the observed pattern (counting statistics). As a compromise between damping the oscillations and computing time, a 12-layer model (Figure 7) was used. A stacking sequence was selected in which $\sum 10L + 01L + 1\bar{1}L + \bar{1}0\bar{L} + 01\bar{L} + \bar{1}1\bar{L}$ changed as little as possible as a function of L. A

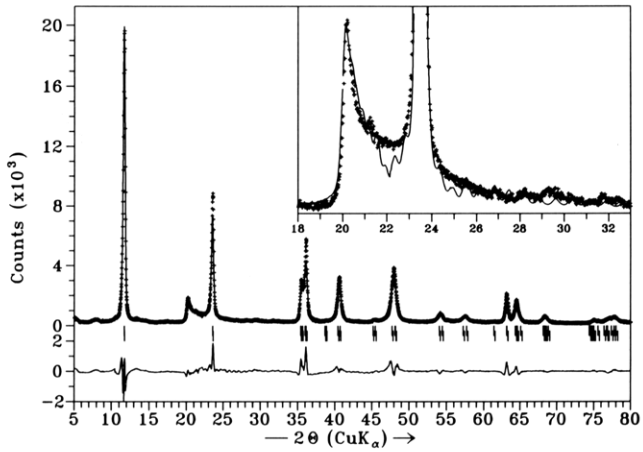

Figure 8. Rietveld refinement of a 12-layer model.

multiple of three layers was used so that the cell can be constrained to hexagonal dimensions ($a = b$, $\alpha = \beta = 90°$, and $\gamma = 120°$). The atomic parameters in different layers were coupled by the coding of the variables.

The next question is the symmetry relationships of the atoms. The atoms within the $[LiAl_2(OH)_6]^+$ layer were initially restricted to D_{3d} symmetry so that only uniform expansion about the lithium cation was allowed. The intralayer bonds are not likely to distort significantly because they are strong compared with hydrogen bonding to the intercalated layer. The atom positions in the intercalated layer were correlated with the $[LiAl_2(OH)_6]^+$ layer immediately above and below. (The shift from one $[LiAl_2(OH)_6]^+$ layer to the next can be in the $-X$, $-Y$, or $X + Y$ direction.) Hydrogen atoms of the $[LiAl_2(OH)_6]^+$ layer were located at a normal crystallographic distance of 0.95 Å above the oxygens but were restricted in X and Y to fractions of $^1/_3$ affecting only the intensity of Bragg reflections where $H^2 + HK + K^2 = 3n$ and $L = 3n$. The hydrogen atoms associated with the intercalated water molecules and hydroxide anion were not included in the model.

The refinement of the 12 layer model shown in Figure 8 is significantly better compared to the refinement of the monoclinic model shown in Figure 6. In the difference profile exhibits some peak shape discrepancies (see Figure 8), noticeable, for example, in the $(11\bar{5})$ and $(11\bar{8})$ Bragg peaks that are calculated to be too narrow and the (300) and (303) calculated to be too wide. Adjustment of atom positions or other refinement variables can reduce the R_w slightly but will not address the discrepancy in peak shape.

Peak Shape. At this point, it is useful to turn to the refinement of the neutron diffraction data. The programs are more versatile and the resolution of the instrument is better. The diffuse scattering owing to disorder which was an important component of the X-ray diffraction pattern is only weakly observed for the $(20L)$ region between the (117) and (118) peaks and can be ignored. Initial refinement of the cell and peak widths were unstable. Small portions of the pattern were analyzed using a Marquet method to fit peak positions, intensities, and widths after the functional form of the TOF refinement programs. The results are listed in Table II. The observed pattern of widths, $\sqrt{\sigma^2_{HKL}}$, increases then decreases with decreasing time-of-flight in contrast to the expected pattern of decreasing widths for a normal material. Anisotropic particle shape or strain can result in a variation of widths. In this partially disordered layered material

Table II. Neutron Powder Data for $LiAl_2(OD)_7{\cdot}2D_2O$

HKL	time (μs)	σ^2_{HKL}	$I_{HKL}/I(t)$
111	26381.2(2)	1703	2946
009	26110.5(3)	2003	1524
$11\bar{2}$	25908.7(6)	1921	735
114	24181.0(5)	2934	976
$11\bar{5}$	23124.2(4)	2901	1179
117	20794.4(39)	1708	51
$11\bar{8}$	19695.1(6)	2446	635
0012	19559.0(30)	830	64
$11\underline{10}$	17572.7(12)	2327	142
$\underline{1111}$	16637.6(64)	1314	17
0015	15645.6(3)	351	166
300	15308.5(1)	182	659
303	15023.2(3)	237	230
1113	14927.8(53)	1652	31
$\underline{306}$	14248.9(25)	418	27
$\underline{11\bar{1}4}$	14165.7(26)	503	28

the anisotropic direction is along the *c* axis. The anisotropy is present to a small degree (compare the $(11\bar{2})$ and (111) to the (009)); however, the peaks appear broadest along the (115) or (118) where such anisotropy does not seem physically reasonable.

The variation in peak shape and width cannot be accounted for by the present model including anisotropy. The variations are due to disorder of the material which was described earlier. However, the simplifying assumption that the shift was exactly $a/3$ based on the position of the Bragg reflection is not correct. That is, the layers are not shifted by exactly $a/3$ form one layer to the next. The shift value differs from $a/3$ but not by a great deal or the refinement would not have progressed as it did.

This can be shown by modelling a very large cell and introducing a slightly increased or decreased staggering. The result is a set of strong peaks spaced by the difference from $^1/_3$ of the shift in fractional coordinates from layer to layer. The separation of these peaks is constant in reciprocal space and so will produce an observed increase in width, Δd, according to eq 4. The fractional shift is

$$\Delta d_{HKL} = d_{HKL}\frac{2Lx + x^2}{(c^2/d^2_{HKL}) + (L + x)^2} \qquad (4)$$

roughly 0.018 (0.1 Å) so that the shift from one layer to the next is not $a/3$ but $a/3 + \delta$ or $a/3 - \delta$, $\delta = 0.018$. The effect is symmetric for the peaks being considered, but not for the line diffraction as demonstrated in Figure 9. Analysis of the (10*L*) indicates that the shift is less than $^1/_3$.

The magnitude of the horizonal shift from layer to layer also determines the size of the model that must be used. That is the number of layers must equal $1/\delta \sim 54$ layers. The deviation in the shift from 1/3 is the origin of the peak shape problem observed in the X-ray refinement. After allowing for the shift between layers into the X-ray model, it is apparent that the broadening effect is larger than for the neutron data because of the hydrothermal treatment of the latter. For samples not subjected to hydrothermal condition, the average deviation of the shift from $^1/_3$ was approximately 0.048. The Rietveld refinement for this model is shown in Figure 10 and the refinement parameters are listed in Table III. Incorporating the fractional shift, δ, the monoclinic parameters are

$$a = a_h,\quad b = a_h\sqrt{3},\quad c = (c_h^2 + a_h^2(^1/_3 + \delta)^2)^{1/2},$$

$$\cos\beta = -(a_h/3c_h) - (\delta a_h/c_h)$$

where a = 5.0972(3) Å, b = 8.8286(5) Å, c = 7.6911(60) Å, β = 101.103(118)° where the large uncertainties in c and β are caused by the error in $\delta = -0.048(3)$. The same model can be rewritten in $C2/m$ as if the stacking disorder was not present (see Table IV).

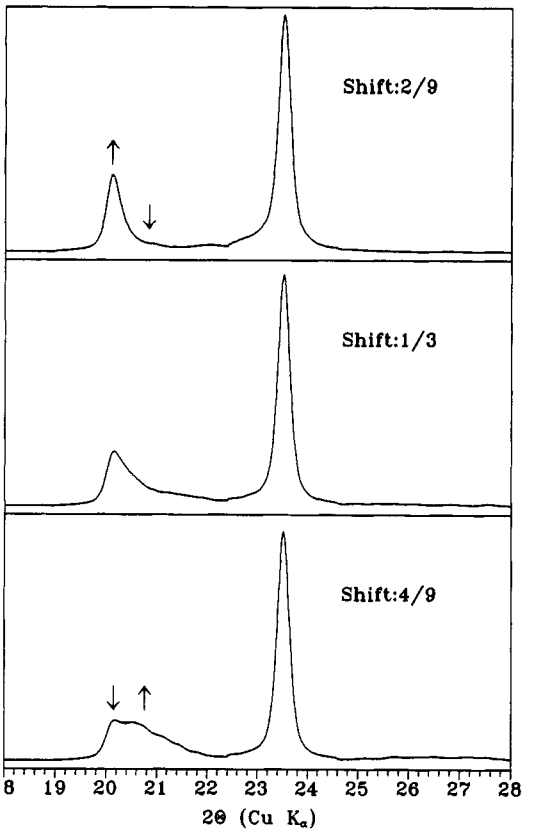

Figure 9. Calculated X-ray diffraction pattern of $LiAl_2(OH)_7{\cdot}2H_2O$ for three values of the shift between the layers.

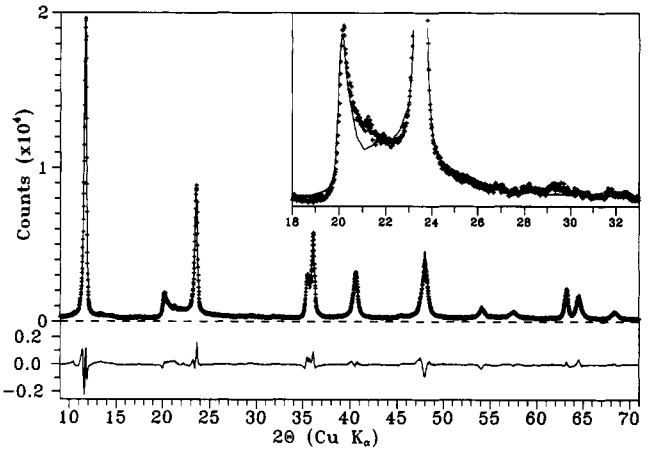

Figure 10. Rietveld refinement of a 54-layer model.

Conclusions

Despite the complexities in the analysis there are two central features of the structure that are important and unambiguous. The cations within each $[LiAl_2(OH)_6]^+$ layer are ordered and the disorder in the structure is simply that although the cations in each layer are ordered their relative positions in successive layers are random. The diffuse scattering is not caused by disorder in packing of the layers or in water/OH^- layer as might have been expected.

Table III. Refined X-ray Rietveld Parameters for a 54-Layer Model

atom	*X*	*Y*	*Z*	*B*	*N*
Li	0	0	0	B_1	1
Al	$^1/_3$	$^2/_3$	0	B_1	1
Al	$^2/_3$	$^1/_3$	0	B_1	1
O(1)	$^1/_3 + \alpha$	0	β/n	B_2	1
O(2)	0	$^1/_3 + \alpha$	β/n	B_2	1
O(3)	$^2/_3 - \alpha$	$^2/_3 - \alpha$	β/n	B_2	1
O(4)	$^2/_3 - \alpha$	0	$-\beta/n$	B_2	1
O(5)	0	$^2/_3 - \alpha$	$-\beta/n$	B_2	1
O(6)	$^1/_3 + \alpha$	$^1/_3 + \alpha$	$-\beta/n$	B_2	1
H(1)	$^1/_3$	0	$\beta + \gamma/n$	2	1
H(2)	0	$^1/_3$	$\beta + \gamma/n$	2	1
H(3)	$^2/_3$	$^2/_3$	$\beta + \gamma/n$	2	1
H(4)	$^2/_3$	0	$-(\beta + \gamma)/n$	2	1
H(5)	0	$^2/_3$	$-(\beta + \gamma)/n$	2	1
H(6)	$^1/_3$	$^1/_3$	$-(\beta + \gamma)/n$	2	
O(7)	$^1/_2 + \delta$	$^1/_2 + \delta$	$^1/_2$	B_3	$^1/_2$
O(7)	$^1/_2 - \delta$	$^1/_2 - \delta$	$^1/_2$	B_3	$^1/_2$
H(7)	$^1/_2 + \epsilon$	$^1/_2 - \epsilon$	$^1/_2$	2	$^1/_2$
H(7)	$^1/_2 - \epsilon$	$^1/_2 + \epsilon$	$^1/_2$	2	$^1/_2$
O(8)	$^1/_6 + \zeta + \eta$	$^5/_6 + \zeta + \eta$	$^1/_2$	B_4	$^1/_2$
O(8)	$^1/_6 + \zeta - \eta$	$^5/_6 + \zeta - \eta$	$^1/_2$	B_4	$^1/_2$
H(8a)	$^1/_6 + \zeta + \eta + \theta_1$	$^5/_6 + \zeta + \eta + \theta_1$	$^1/_2$	2	$^1/_2$
H(8b)	$^1/_6 + \zeta + \eta + \theta_2$	$^5/_6 + \zeta + \eta + \theta_1$	$^1/_2$	2	$^1/_2$
H(8a)	$^1/_6 + \zeta - \eta + \theta_1$	$^5/_6 + \zeta - \eta + \theta_2$	$^1/_2$	2	$^1/_2$
H(8b)	$^1/_6 + \zeta - \eta + \theta_2$	$^5/_6 + \zeta - \eta + \theta_1$	$^1/_2$	2	$^1/_2$
O(9)	$^5/_6 - \zeta + \eta$	$^1/_6 - \zeta + \eta$	$^1/_2$	B_4	$^1/_2$
O(9)	$^5/_6 - \zeta - \eta$	$^1/_6 - \zeta - \eta$	$^1/_2$	B_4	$^1/_2$
H(9a)	$^5/_6 - \zeta + \eta + \theta_1$	$^1/_6 - \zeta + \eta - \theta_2$	$^1/_2$	2	$^1/_2$
H(9b)	$^5/_6 - \zeta + \eta + \theta_2$	$^1/_6 - \zeta + \eta - \theta_1$	$^1/_2$	2	$^1/_2$
H(9a)	$^5/_6 - \zeta - \eta + \theta_1$	$^1/_6 - \zeta - \eta - \theta_2$	$^1/_2$	2	$^1/_2$
H(9b)	$^5/_6 - \zeta - \eta + \theta_2$	$^1/_6 - \zeta - \eta - \theta_1$	$^1/_2$	2	$^1/_2$

hydrogen parameters set at $\gamma = 0.95$ Å, $\theta_1 = 0.0806$, $\theta_2 = 0.2136$, $\epsilon = 0.1$

$\alpha = 0.0291$ (7), $\beta = 0.129$, $\delta = 0.166$ (3), $\zeta = 0.011$ (4), $\eta = 0.086$ (4)

$B_1 = 0.7(1)$, $B_2 = -0.3(1)$, $B_3 = 4(1)$, $B_4 = -2.2(2)$

$a = 5.0972(3)$ Å, $c = 7.5524(9)\cdot 54$, slide $= ^1/_3 - 0.048(3)$, $n = 54$

54-layer stacking sequence:

112100001111202111220110012000220202211021202120102 22

$R_p = 10.85$, $R_{wp} = 13.58$

Table IV. The 54-Layer Model Transformed into *C*2/*m* If No Stacking Disorder Were Present

atom	site	*X*	*Y*	*Z*	*B*	*N*
Li	2*a*, 2/*m*	0	0	0	0.7	1
Al	4*g*, 2	0	$^1/_3$	0	0.7	1
O(1)	8*j*, 1	0.2820	0.3188	0.129	−0.3	1
O(2)	4*i*, *m*	0.2675	0	0.129	−0.3	1
H(1)	8*j*, 1	0.26066	$^1/_3$	0.255	2	1
H(2)	4*i*, *m*	0.26066	0	0.255	2	1
O(7)	4*i*, *m*	0.334	0	$^1/_2$	4	$^1/_2$
H(7)	4*h*, 2	$^1/_2$	0.1	$^1/_2$	2	$^1/_2$
O(8)	8*j*, 1	0.339	0.414	$^1/_2$	−2.2	$^1/_2$
H(8a)	8*j*, 1	0.405	0.561	$^1/_2$	2	$^1/_2$
H(8b)	8*j*, 1	0.405	0.267	$^1/_2$	2	$^1/_2$

$a = 5.0972(3)$ Å, $b = 8.8286(5)$ Å, $c = 7.6911(60)$ Å, $\beta = 101.103(118)°$

This structural behavior has implications for the use of this material and other layered double hydroxides.[28] Catalytic properties are primarily the result of local environments, and while long range disorder complicates the analysis it does not present a serious problem for the application of these materials. Disorder can have a direct affect on other properties and applications. For example, Dutta et al.[29] have reported the onset of nonlinear optical behavior in an intercalated lithium dialuminate. Second-order harmonic generation depends on the degree of alignment in a noncentric environment and disorder is generally detrimental. Long-range ordering of the layers and associated intercalated species is required for efficient nonlinear optical properties and an effective synthesis will have to address ways of achieving this effect.

Acknowledgment. The authors gratefully acknowledge support from the National Science Foundation, Solid State Chemistry, Contract DMR-89-15897. We also thank the Northwestern Materials Research Center for support of the X-ray Diffraction Facility, MRL-DMR-8821571 and the Intense Pulsed Neutron Source at Argonne National Laboratory, US Department of Energy under Contract W-31-109-ENG-38.

(28) Wang, J.; Tian, Y.; Wang, R.-C.; Clearfield, A. *Chem. Mater.* **1992**, *4*, 1276.

(29) Cooper, S.; Dutta, P. *J. Phys. Chem.* **1990**, *94*, 114.